Electronic structure of cerium monopnictides under pressure

1998 J. Phys.: Condens. Matter 10 5309

(http://iopscience.iop.org/0953-8984/10/24/009)

J. Phys.: Condens. Matter **10** (1998) 5309–5325. Printed in the UK PII: S0953-8984(98)91910-5

Electronic structure of cerium monopnictides under pressure

A Svane†, Z Szotek‡, W M Temmerman‡, J Lægsgaard† and H Winter§

† Institute of Physics and Astronomy, University of Aarhus, DK-8000 Aarhus C, Denmark

‡ Daresbury Laboratory, Warrington WA4 4AD, UK

§ Forschungszentrum Karlsruhe, INFP, Postfach 3640, D-7500 Karlsruhe, Germany

Received 19 February 1998

Abstract. The electronic structures of the cerium monopnictides CeN, CeP, CeAs, CeSb and CeBi are calculated within the self-interaction-corrected local-spin-density approximation. This method allows for a description of the Ce f electrons as either localized or delocalized, thus providing a unified scheme to describe the large-volume ground states characterized by trivalent Ce ions as well as the low-volume high-pressure phases with tetravalent Ce ions. The structural phase transitions observed in CeP, CeAs, CeSb and CeBi are well described within this theory, as are the antiferromagnetic structures and semimetallic characteristics. The trends of the series may be understood in terms of the increasing localization of the f electron with increasing nuclear charge of the ligand.

1. Introduction

Cerium compounds exhibit a wide range of physical properties including heavy-fermion, mixed-valence and Kondo insulator behaviour. These phenomena are intimately connected with the strong correlations among the Ce f electrons, and the proper theoretical description of these remains a challenge. The cerium monopnictides CeN, CeP, CeAs, CeSb and CeBi constitute a class of relatively simple cerium-based systems, in which systematic studies of the f-electron correlations may be undertaken, which is the purpose of the present paper.

The interaction between the f electrons and the conduction electrons varies with the interatomic distance, and as a consequence the cerium monopnictides have peculiar properties as a function of applied hydrostatic pressure. At ambient conditions they all crystallize in the rock-salt (B1) crystal structure. With the exception of the case for CeN, the lattice constants indicate a trivalent nature of the Ce ions [1]. CeN is closer to a tetravalent Ce configuration, as supported by both photoemission experiments [2–5] and analysis of optical absorption [6]. Thus, CeN is similar to the collapsed α-phase of pure cerium, where the cerium f electron contributes actively to the cohesive properties, while the other Ce monopnictides at ambient conditions are more similar to the γ-phase of cerium, which is characterized by 'localized', i.e. atomic-like, f electrons. When pressure is applied, discontinuous structural phase transitions occur [1, 7–12], again with the exception of the case for CeN, for which to the best of our knowledge no pressure experiment has been reported. In CeP a peculiar *isostructural* transition is observed at a pressure of $P_1 \sim 90$ kbar accompanied by a volume collapse of $\Delta V_1 \sim 3\%$ [7] (at 300 K—at low temperature the transition pressure has been determined to be 55 kbar [8]). This transition is similar in appearance to the isostructural $\alpha \rightarrow \gamma$ phase transition in cerium metal, and is usually

0953-8984/98/245309+17$19.50

attributed to a change from trivalent to tetravalent behaviour of the cerium ions. At a higher pressure of $P_2 \sim 150 \pm 40$ kbar [13], a second transition to the CsCl (B2) structure is observed, with a volume collapse of $\Delta V_2 \sim 10\%$ [7]. In CeAs, a single B1 $\rightarrow$ B2 phase transition occurs at a pressure of $P \sim 140 \pm 20$ kbar with a volume collapse of $\Delta V \sim 11\%$ [9]. Some authors have claimed that no substantial change in Ce valency occurs at the transition [9], while others conclude that there is a significant change [10]. In CeSb and CeBi, high-pressure tetragonal phases are observed, at $P = 80 \pm 20$ kbar and $P = 90 \pm 40$ kbar, respectively, with volume collapses of $\Delta V \sim 10\%$ [11] in CeSb and $\Delta V \sim 8\%$ [12] in CeBi. The tetragonal phase may be viewed as a uniaxial compression of the CsCl structure along the 001 direction with a c/a ratio of 0.82 in CeSb [11] and 0.84 in CeBi [12]. In both cases the Ce ions are concluded to remain trivalent across the phase transition.

The magnetic properties of the cerium monopnictides (again excluding CeN) are quite complicated with several antiferromagnetically ordered phases, including a devil's staircase, and phase transitions as a function of pressure, temperature and applied magnetic field [8, 14–17]. For CeP and CeAs the ground-state configuration in zero field and at zero pressure and temperature is the AF1 structure, which consists of an antiferromagnetic stacking of (100) planes, within which the Ce spins are ferromagnetically coupled. In CeSb and CeBi the stacking of ferromagnetically ordered (100) planes follows the sequence $(++--)$ (AF1A). The Néel temperatures are quite low for all of the cerium monopnictides, 8–30 K [18], indicating small exchange-coupling parameters, and at high temperatures their susceptibilities show characteristic Curie–Weiss behaviour indicative of independent local moments. Only CeN behaves more as a Pauli enhanced paramagnet.

The Ce monopnictides are low-carrier-density strongly correlated electron systems [19]. With the exception of CeN, they all show semi-metallic behaviour with carrier concentrations of 0.1%, 0.24%, 2.1% and 2.9% per formula unit, in CeP, CeAs, CeSb and CeBi, respectively [18, 20–22]. From de Haas–van Alphen measurements it is inferred that the Fermi surface is characterized by small hole pockets around the Γ point and small electron pockets around the M point [23, 24]. This Fermi surface topology is also consistent with recent high-resolution angle-resolved photoemission studies of CeBi [25] and of CeP [26].

In the present work we will undertake a systematic theoretical investigation of the Ce monopnictides using *ab initio* electronic structure methods based on the self-interaction-corrected (SIC) local-spin-density (LSD) approximation [27]. In this scheme the Ce f electrons may be described as either localized or delocalized [28], thus mimicking the trivalent and tetravalent Ce atomic configurations, respectively. It will be demonstrated that this approach can account for the fascinating structural, magnetic and semi-metallic properties of these systems. A preliminary account of this work has recently been published [29].

Previous theoretical investigations of the electronic structure of the cerium monopnictides have focused on aspects other than those considered in the present work. Hasegawa [30] performed augmented-plane-wave calculations for lanthanum monopnictides and noted a close resemblance to the valence electron photoemission spectra of the corresponding Ce monopnictides. Norman *et al* [31] obtained quantitative agreement with photoemission experiments by performing supercell calculations for the photoexcited solid and assuming either a poorly screened localized 4f hole or a fully screened delocalized 4f hole. The magneto-optical properties of CeSb have been the subject of several theoretical studies based upon the LSD or the LDA $+ U$ methods [32–35]. The LDA $+ U$ method is similar in spirit to the SIC-LSD method used in the present work in producing an orbital

polarization among the f electrons and a Coulomb correlated splitting between occupied and unoccupied f-electron states. This removes the significant f-electron contribution to the density of states at the Fermi level which occurs in the LSD approximation and one obtains the observed semi-metallic CeSb, and a significant increase in magnetic anisotropy.

In section 2 a short account is given of the SIC-LSD approach, while section 3 presents the results of the structural studies. Section 4 is devoted to the magnetic studies of CeP, and in section 5 we discuss the electronic band structure and density of states of CeP. Section 6 concludes this work.

2. The SIC-LSD formalism

The self-interaction-corrected local-spin-density approximation [27] is an *ab initio* electronic structure scheme, which is capable of describing localization phenomena in solids [36–40, 28]. In this scheme the spurious self-interaction of each occupied electron state is subtracted from the conventional LSD approximation to the total-energy functional, which leads to a greatly improved description of static Coulomb correlation effects over the LSD approximation. This has been demonstrated in studies of the Hubbard model [41–44], in applications to 3d monoxides [36, 37, 45] and La_2CuO_4 [46, 47], f-electron systems [48, 38–40, 49, 50] and hydrogen solid [51].

In the LSD approximation the total energy of a many-electron system is found as the minimum of an energy functional, which approximates the exchange and correlation effects by a simple expression:

$$E_{xc}^{LSD}[\bar{n}] = \int \epsilon_{xc}^{hom}(\bar{n}(\boldsymbol{r}))n(\boldsymbol{r})\ \mathrm{d}^3r \tag{1}$$

where $\bar{n}$ is the total electron spin density of the system:

$$\bar{n}(\boldsymbol{r}) = (n^{\uparrow}(\boldsymbol{r}), n^{\downarrow}(\boldsymbol{r}))$$

and

$$n(\boldsymbol{r}) = n^{\uparrow}(\boldsymbol{r}) + n^{\downarrow}(\boldsymbol{r})$$

and $\epsilon_{xc}^{hom}(\bar{n})$ is the exchange–correlation energy density of a homogeneous electron gas at spin density $\bar{n}$ [52, 53]. The exact exchange–correlation energy functional, E_{xc}, of density functional theory has the property that for *any* single-electron density, $\bar{n}_\alpha$, it exactly cancels the static Coulomb interaction energy for that density:

$$U[n_\alpha] + E_{xc}[\bar{n}_\alpha] = 0 \tag{2}$$

where

$$U[n] = \int\int \frac{n(\boldsymbol{r})n(\boldsymbol{r}')}{|\boldsymbol{r}-\boldsymbol{r}'|}\ \mathrm{d}^3r\ \mathrm{d}^3r'. \tag{3}$$

Atomic rydberg units ($\hbar = 2m_e = e^2/2 = 1$) are used throughout.

The cancellation in equation (2) is not complete in the LSD approximation, and the residual

$$\delta_\alpha = U[n_\alpha] + E_{xc}^{LSD}[\bar{n}_\alpha] \tag{4}$$

is interpreted as the self-interaction of the electron in state ψ_α.

Perdew and Zunger [27] suggested constructing a self-interaction-free total-energy functional by subtracting the self-interaction of each occupied electron state from the LSD total-energy functional, which defines the SIC-LSD total-energy functional:

$$E^{SIC}[\{\psi_\alpha\}] = \sum_\alpha \langle\psi_\alpha|-\Delta|\psi_\alpha\rangle + U[n] + E_{xc}^{LSD}[\bar{n}] + V_{ext}[n] - \sum_\alpha \delta_\alpha. \tag{5}$$

Here, $U[n]$ and $E_{xc}^{LSD}[\bar{n}]$ are defined in equations (3) and (1), while $V_{ext}[n]$ denotes the energy of the interaction with the lattice of ions:

$$V_{ext}[n] = \int V_{ext}(\boldsymbol{r})\ n(\boldsymbol{r})\ \mathrm{d}^3r. \tag{6}$$

As expressed in equations (1)–(6), E^{SIC} appears to be a functional of the set of occupied orbitals rather than of the total spin density only, like E^{LSD}. By a reformulation it may be shown [27, 54] that E^{SIC} can in fact be regarded as a functional of the total spin density only. The associated exchange–correlation energy functional $E_{xc}^{SIC}[\bar{n}]$ is, however, only implicitly defined [54], for which reason it is rather impractical to exploit the associated Kohn–Sham equations. For periodic solids the *SIC-LSD approximation is a genuine extension of the LSD approximation* in the sense that the self-interaction correction is only finite for localized states, which means that for Bloch-like single-particle states E^{SIC} coincides with E^{LSD}. Therefore, the LSD minimum is also a local minimum of E^{SIC}. In some cases another set of single-particle states may be found, not all being in Bloch form, to provide a local minimum for E^{SIC}. For this to happen some states must exist which can benefit from the self-interaction term without losing too much band formation energy. This will usually be the case for rather well localized states like the 3d states in transition metal oxides or the 4f states in rare-earth compounds. Thus, E^{SIC} is a density functional, which may be used to describe localized as well as delocalized electron states. As we will demonstrate in the following, the relative position of the two minima may be influenced by external parameters such as hydrostatic pressure allowing a localization $\rightarrow$ delocalization transition to occur.

In the present work two different, yet equivalent, implementations of the SIC-LSD approach have been used [28, 55, 38]. Both are based on the linear muffin-tin orbital (LMTO) method [56, 57], i.e., the electronic wave functions are expanded in terms of muffin-tin orbitals, and the minimization of E^{SIC} becomes a non-linear minimization problem in the expansion coefficients. The atomic sphere approximation (ASA) is used, according to which the polyhedral Wigner–Seitz cell is approximated by slightly overlapping atom-centred spheres with a total volume equal to the actual crystal volume. Inside each sphere the potential is assumed spherically symmetric. To improve the packing of the NaCl structure, additional empty spheres are introduced at high-symmetry interstitial sites. The accuracy of the ASA is explored in the following section by comparison with results obtained using a full-potential version of the LMTO method [58]. Care has been taken to converge the calculations with respect to the number of $\boldsymbol{k}$-vectors, using 525 and 455 $\boldsymbol{k}$-points in the irreducible Brillouin zone of the NaCl and CsCl structures, respectively. Likewise, the inclusion of the Ce 5p states as band states is crucial for getting an accurate evaluation of the total energy. While energetically deep (about 1.5 Ryd below the Fermi level), the 5p states have a radial extension greater than that of the 4f state. Consequently, changes in 4f occupation have a large effect on the shape of the 5p wave functions, which may no longer be treated in the frozen-core approximation. This relaxation of the 5p states has been done both using a separate energy window (a two-panel calculation) and by including the 5p states as normal valence states.

Table 1. Theoretical and experimental equilibrium lattice constants and bulk moduli for the cerium monopnictides. The crystal structure is in all cases NaCl (B1) and is described with one localized f electron per Ce atom, with the exception of the case for CeN, for which all f electrons are itinerant.

	A (Å)		*B* (kbar)	
	Theory	Experiment[a]	Theory	Experiment
CeN	4.87	5.01	1590	—
CeP	5.91	5.90	892	640[b]
CeAs	6.04	6.06	844	690[c]
CeSb	6.36	6.40	692	715[d]
CeBi	6.56	6.49	618	496[e]

[a] Reference [59].
[b] Reference [7].
[c] Reference [9].
[d] Reference [11].
[e] Reference [12].

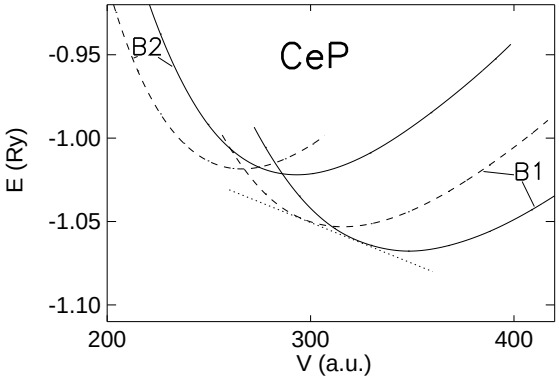

Figure 1. The cohesive energy of CeP (in Ryd/formula unit) as a function of the specific volume (in a_0^3/formula unit). Two crystal structures, the B1 and the B2, are considered, and each with two different treatments of the Ce f electrons. The full curves correspond to calculations with one localized f electron per Ce atom, while the dashed curves correspond to itinerant f electrons. The dotted line marks the common tangent at the isostructural phase transition.

3. Structural studies

The results of the present structural calculations are presented in figures 1–7 with the equilibrium volume parameters quoted in table 1. In all of the calculations presented in this section a ferromagnetic structure is assumed. This is only done for computational simplicity. In the next section it will be shown that our calculations do obtain the correct AF1 ground state, the energy of the ferromagnetic structure being only 1 mRyd/formula unit higher than the ground-state energy.

3.1. CeP

The total energy as a function of volume for CeP was calculated for each of the phases B1 and B2 and with the f electron treated as either delocalized (LSD) or localized (SIC-LSD). The results are shown in figure 1. The lowest energy is found in the B1 phase with localized

f electrons and with a specific volume of 348 a_0^3 per formula unit, which coincides with the experimental equilibrium volume. The calculated bulk modulus of 892 kbar is, however, larger than the experimental value by 40%. The B1 phase with delocalized f electrons has its minimum at a considerably lower volume (due to the significant f-electron band formation energy providing a large negative component to the pressure). From the common tangent a phase transition is predicted at a pressure of 71 kbar with a volume collapse of $\Delta V/V_0 = 8\%$. The experimental B1 $\rightarrow$ B1 phase transition occurs at room temperature at a pressure of 90 kbar with a volume collapse of 3% [7], but resistivity measurements at low temperature show the transition to occur at 55 kbar [8]. The present calculated transition pressure is thus in excellent agreement with experiment. The B2 structure is not as favourable for the CeP compound, since the calculated energy is substantially higher than that of the B1 structure. This holds for both localized and delocalized f electrons. From figure 1 we conclude that the B2 structure with localized f electrons is never reached in CeP, while at high pressure a second phase transition to the B2 structure with delocalized f electrons is found. The transition pressure is calculated to be 113 kbar and the volume collapse 12%, while experimentally the B1 $\rightarrow$ B2 phase transition occurs at 150 ± 40 kbar [13]. The experimental volume collapse is 10%. Some uncertainty is associated with comparing the total energies calculated for the B1 and B2 phases in the ASA, since empty spheres were used for the B1 structure but not for the B2 phase. Therefore we have also investigated the high-pressure transition in CeP with the full-potential LMTO method [58], where no problem of this sort occurs. In this case we have found a transition pressure of 167 kbar, which is somewhat higher, but in good accord with the experimental value. The reliability of the ASA is further discussed in subsection 3.3.

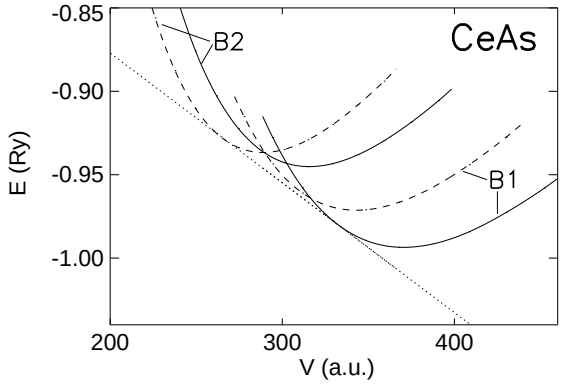

Figure 2. The cohesive energy of CeAs (in Ryd/formula unit) as a function of the specific volume (in a_0^3/formula unit). Two crystal structures, the B1 and the B2, are considered, and each with two different treatments of the Ce f electrons. The full curves correspond to calculations with one localized f electron per Ce atom, while the dashed curves correspond to itinerant f electrons. The dotted line marks the common tangent at the phase transition.

3.2. CeAs

The calculated total-energy curves for CeAs are shown in figure 2. Similarly to the case for CeP, four different cases have been considered, the B1 or B2 structures with localized or delocalized f electrons. The zero-pressure ground state is found to be the B1 structure with localized f electrons. The equilibrium volume is found to be 371 a_0^3 with a bulk modulus of

844 kbar. This compares favourably with the experimental values of 375 a_0^3 and 690 kbar. The relative placement of the four curves is qualitatively the same as is found for CeP, but the small differences have important implications. In comparison with CeP, for CeAs the total-energy curves of the localized phases are slightly lowered with respect to the total-energy curves of the delocalized phases, which is caused by the somewhat larger specific volume due to the larger ligand ion. As a consequence, the common-tangent construction leads to only one phase transition, from the localized B1 structure directly to the delocalized B2 structure. The transition pressure is calculated to be 114 kbar with an 18% volume collapse. This is in accord with an experimental situation, where a B1 $\rightarrow$ B2 transition is observed at 140 ± 20 kbar, with a volume collapse of 11%. There has been some dispute over the nature of the f electrons in the high-pressure phase [9, 10]. The present calculations do not find localized f electrons in the B2 phase of CeAs. This conclusion cannot be taken too literally, however, since the theoretical pictures offered by the present work are rather idealized. In reality, the ground state of CeAs at a given pressure and temperature will be a complicated fluctuating mixture of localized and delocalized f electrons. The fact that the B1 phase with delocalized f electrons is very close to the transition line may imply that the B1 phase at pressures just below the transition line attains a significant component of delocalized f-electron character, i.e., mixed-valence behaviour. We take the present calculations as evidence for the high-pressure phase having *predominantly* delocalized f electrons, though.

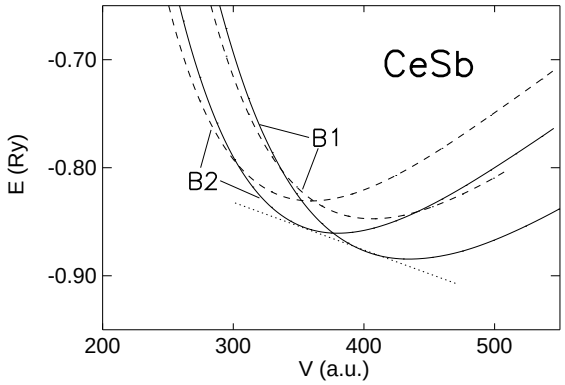

Figure 3. The cohesive energy of CeSb (in Ryd/formula unit) as a function of the specific volume (in a_0^3/formula unit). Two crystal structures, the B1 and the B2, are considered, and each with two different treatments of the Ce f electrons. The full curves correspond to calculations with one localized f electron per Ce atom, while the dashed curves correspond to itinerant f electrons. The dotted line marks the common tangent for the first structural phase transition.

3.3. CeSb

Figure 3 shows the calculated energy–volume curves for the B1 and B2 structures with either localized or delocalized f electrons. The equilibrium volume is calculated to be 435 a_0^3, which is 1.5% lower than the experimental value of 442 a_0^3. The bulk modulus is calculated to be 692 kbar while the experimental value is 715 kbar. Comparing with CeP and CeAs it is seen that for CeSb the localized phases are further stabilized with respect to the delocalized phases. As a consequence, the first transition to occur is from B1 with localized f electrons to B2 with localized f electrons. The transition pressure is found to be 70 kbar, while the experimental B1 $\rightarrow$ B2 (distorted) transition occurs at 85 ± 25 kbar, i.e. with increasing

pressure the transition is observed at 110 kbar, while on releasing the pressure, the reverse transition is seen at 60 kbar. The calculated volume collapse of 11% compares favourably with the 10% volume difference between the two phases seen at 85 kbar in the hysteresis loop. From figure 3 it is seen that a second isostructural B2 $\rightarrow$ B2 transition is predicted to occur at high pressure, at 252 kbar, where the f electrons are delocalizing. The associated volume collapse is 4%. Experimentally, CeSb has been investigated up to 250 kbar [11], but only one discontinuous phase transition was observed. It seems necessary to investigate CeSb at somewhat higher pressures to clarify whether a second phase transition occurs. From the present work we cannot exclude the possibility of there being a new structure (i.e., neither B1 nor B2) on the high-pressure side of a possible second phase transition.

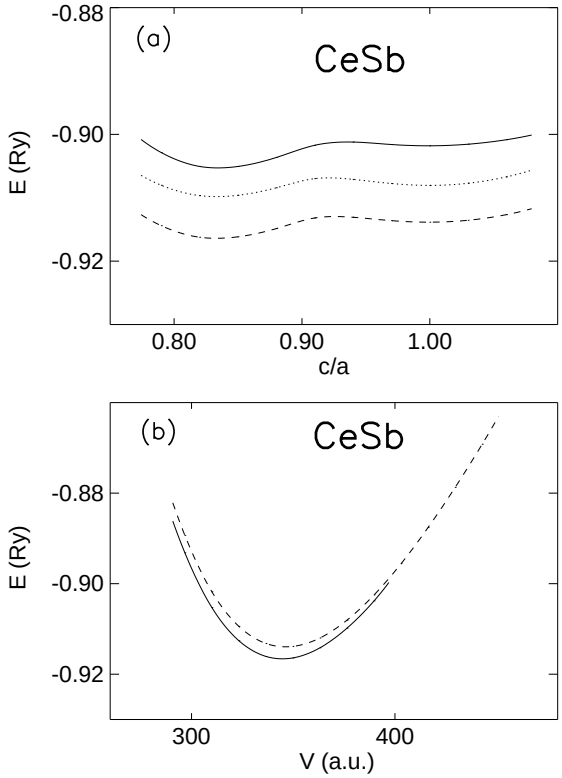

Figure 4. (a) The total energy as a function of the c/a ratio in the tetragonal phase of CeSb, calculated with the full-potential LMTO method. The units are as in figure 1. Calculations for $V/V_0 = 0.70$ (full curve), 0.79 (dashed curve) and 0.85 (dotted curve), where $V_0 = 442a_0^3$, are shown. The ideal CsCl (B2) structure corresponds to $c/a = 1.0$. (b) The full-potential LMTO cohesive energy versus the volume for CeSb in the ideal (dashed curve) and distorted (full curve) B2 structures. The units are as in figure 1.

To investigate the importance of the distortion of the B2 structure in the high-pressure phase of CeSb, we have computed the total energy with the full-potential LMTO method in the tetragonal structure as a function of volume and the c/a ratio, the latter varying in the range from 0.79 to 1.06. The case of $c/a = 1$ corresponds to the B2 structure. Figure 4(a) shows a few examples of our results, which may be summarized as follows. At a particular volume (in the range 0.70 V_0 to 0.88 V_0, where V_0 is the experimental zero-pressure equilibrium volume, $V_0 = 442\ a_0^3$) the total energy as a function of c/a exhibits

two minima, one at $c/a = 0.833$–0.835 and the second at $c/a = 1.0$, i.e. at the B2 value. The former has in all cases the lowest energy, but the latter minimum is only a few mRyd higher, so the two minima are in fact almost degenerate. The experimental c/a ratio is 0.82, which is in perfect agreement with the present calculations. Figure 4(b) shows the comparison of the energy of the two minima. The volumes of the minima of the two curves differ by less than 0.5%. We conclude that, on the scale of the energies in figure 3, i.e. relevant for the discussion of the structural phase transitions, the B2 structure may be regarded as representative for the high-pressure phase, even if the experimental structure is the distorted B2 structure. Quite similar results have been found for CeBi and CeAs, the only difference being that for CeBi the energy minimum corresponding to the distorted B2 structure is noticeably lowered, while for CeAs the minimum corresponding to the undistorted B2 structure is lowest, in accordance with experiment. At the minimum of the total-energy curve the energy differences between the undistorted and distorted B2 structure are -7.9 mRyd, $+2.7$ mRyd and $+4.4$ mRyd in CeAs, CeSb and CeBi, respectively.

A second question to consider is whether the ASA is sufficiently accurate for calculating the total energy to the required precision. As already mentioned, due to its complexity the

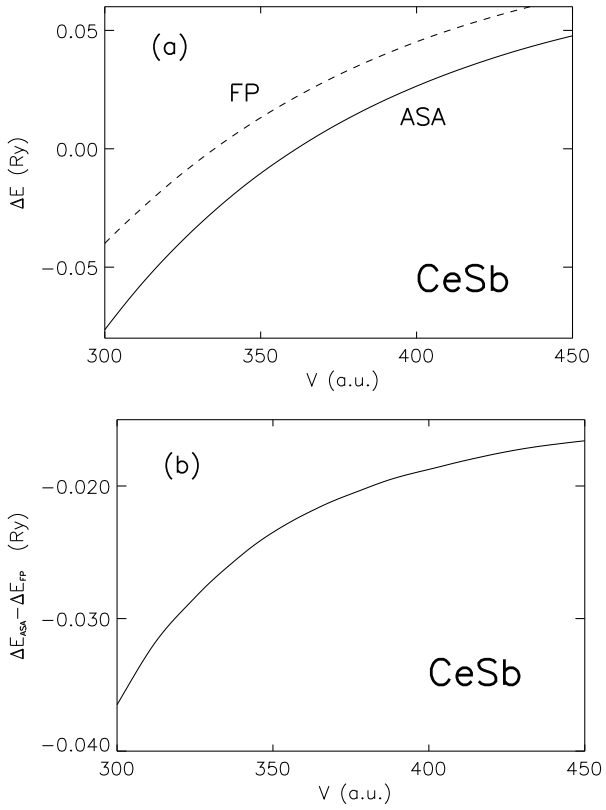

Figure 5. (a) The total-energy difference, $\Delta E = E_{B2} - E_{B1}$, between the B2 and B1 structures of CeSb as a function of volume, as calculated with the ASA LMTO (full curve) and with the full-potential LMTO (dashed curve) methods. The units are as in figure 1. (b) The difference between the ASA structural energy difference and the full-potential structural energy difference. The units are as in figure 1. The negative sign of the energy difference implies that the ASA calculations find the B2 structure to be too low in energy compared to the B1 structure.

SIC-LSD approximation has only been implemented with the ASA, so for consistency, in comparing structures with localized and delocalized f electrons, the ASA has to be used. The filling of space with atomic spheres is, however, rather different in the B1 and B2 structures, so it is not clear that total energies calculated under the ASA are directly comparable in the two structures. When empty spheres are introduced into the B1 structure, the sphere centres constitute a bcc lattice, which is also the case for the centres of atomic spheres in the B2 structure. The values chosen for the sphere radii may, however, not be identical for the two phases. To investigate the influence of the ASA we calculated the total-energy difference between the B1 and B2 phases with the ASA and with the full-potential LMTO method, the latter (to a high degree) being independent of the choice of sphere radii. Figure 5(a) shows the energy difference $\Delta E = E_{B2} - E_{B1}$ as calculated in these two approximations, while figure 5(b) depicts the error in this structural energy difference due to the ASA: $(E_{B2} - E_{B1})_{FP} - (E_{B2} - E_{B1})_{ASA}$. In the volume range 300–400 a_0^3 the energy difference is between 20 and 36 mRyd. This is a significant ASA error, which renders the calculated transition pressures for those transitions that go from B1 to B2 somewhat uncertain, the trend for the pure ASA calculations to underestimate the transition pressures. If we can assume that the correction of figure 5(b) can be taken over to the calculation with localized f electrons, the transition pressures should be somewhat higher in a full-potential treatment than in the ASA. It is, however, not obvious that such a correction is applicable, and we prefer to quote the pure ASA results with appropriate caution.

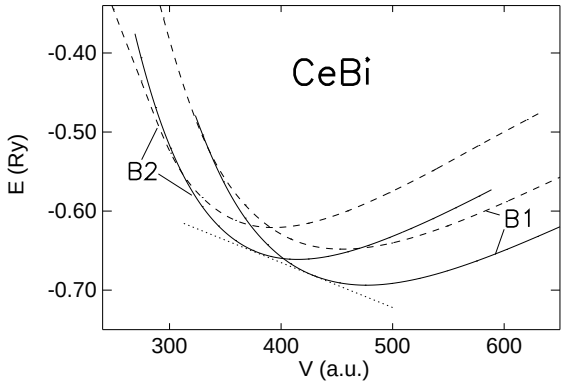

Figure 6. The cohesive energy of CeBi (in Ryd/formula unit) as a function of the specific volume (in a_0^3/formula unit). Two crystal structures, the B1 and the B2, were considered, and each with two different treatments of the Ce f electrons. The full curves correspond to calculations with one localized f electron per Ce atom, while the dashed curves correspond to itinerant f electrons. The dotted line marks the common tangent at the first structural phase transition.

3.4. CeBi

Figure 6 shows the total energy of CeBi as calculated for the B1 and B2 structures with the f electrons treated as either localized or delocalized. In view of the discussion of the previous subsection, we render the total energy of the B2 phase representative of that of the distorted tetragonal structure. From our LDA full-potential LMTO study we have found a modest 4.4 mRyd energy difference between the ideal and distorted B2 structures. The calculated c/a ratio for the distorted structure is found to be 0.832, which compares excellently with the experimental c/a ratio of 0.84. The trends observed in going from CeP

to CeAs to CeSb are seen to continue in CeBi, namely a preference for localized f electrons in both the B1 and the B2 phases. A transition from B1 to B2 is found at a pressure of 88 kbar with a volume collapse of 9%, which is in perfect accord with the experimentally observed transition at 90 ± 40 with a volume collapse of 9%. As in CeSb, both sides of the transition are characterized by localized f electrons. Only at a high pressure of ∼370 kbar is a delocalization transition foreseen, as for CeSb, with a good chance of being isostructural. The calculated equilibrium volume is 477 a_0^3, which is 3.5% higher than the experimental equilibrium volume. The bulk modulus is 618 kbar, which is somewhat too high compared to the experimental value of 496 kbar [12].

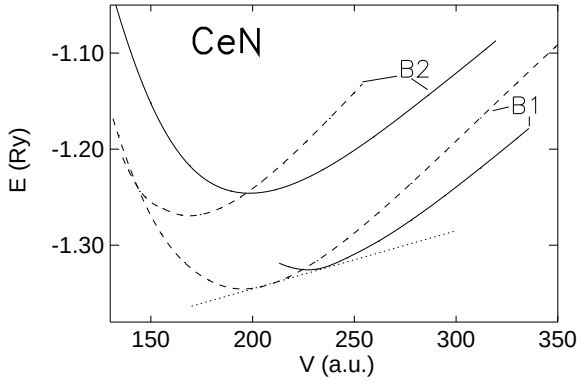

Figure 7. The cohesive energy of CeN (in Ryd/formula unit) as a function of the specific volume (in a_0^3/formula unit). Two crystal structures, the B1 and the B2, were considered, and each with two different treatments of the Ce f electrons. The full curves correspond to calculations with one localized f electron per Ce atom, while the dashed curves correspond to itinerant f electrons. The dotted line marks the common tangent corresponding to a hypothetical negative pressure isostructural phase transition.

3.5. CeN

The total energy of CeN as a function of volume is shown in figure 7 with both the B1 and B2 structures considered and with the f electrons treated as either localized or delocalized. In contrast to the case for the other cerium monopnictides the localization of the f electrons is never favoured in CeN. The equilibrium structure is the B1 structure with a volume of 195 a_0^3 and a bulk modulus of 1590 kbar. The experimental volume is 212 a_0^3. The slight underestimation of the equilibrium volume may be an indication that the true CeN ground state is of a more complicated structure than that of itinerant f electrons. The present calculations show, however, that the LDA ground state with itinerant f electrons is a better representative of the CeN ground state than the SIC-LSD ground state with fully localized f electrons. The present work predicts a structural phase transition B1 $\rightarrow$ B2 at around 620 kbar. To the best of our knowledge, no experimental information on CeN under pressure has been reported. The transition from the delocalized to the localized phase may take place at a negative pressure of $P = -111$ kbar, i.e., at expanded volume. Such negative pressure could be mimicked experimentally by alloying, replacing either N with P or Ce with La. We are not aware that any such experiments have been reported. Alternatively, the transition could occur at high temperature, since the localized phase has a considerable entropy, $S \sim k_B \ln 6$, due to the localized Ce moments ($j = 5/2$). From the energy difference between the minima of the localized and delocalized B1 structure, we may roughly estimate

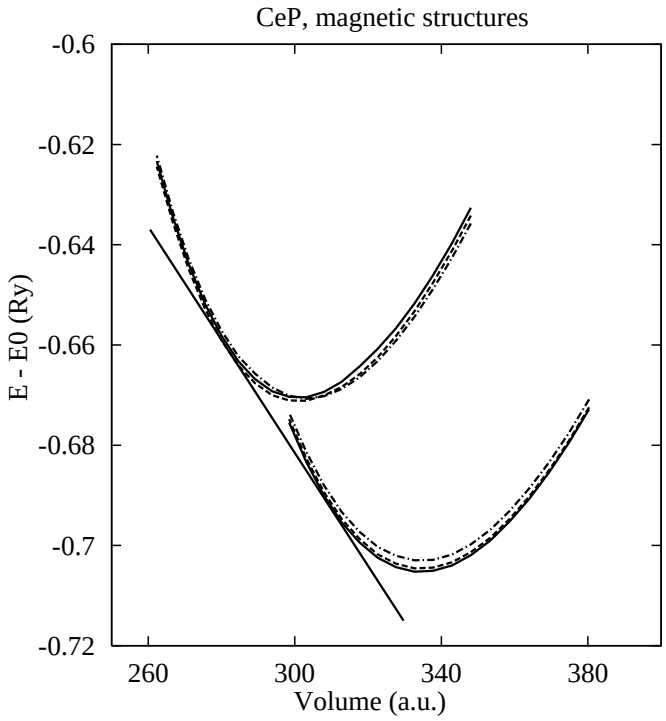

Figure 8. The total energy of CeP (in Ryd/formula unit) as a function of the specific volume (in a_0^3/formula unit) in the B1 crystal structure with three different magnetic structures: AF1 (solid curves), AF2 (dashed curves) and ferromagnetic (chain curves). The lower set of curves corresponds to the calculations treating one Ce f electron as localized, whilst the upper set refers to the calculations with a delocalized f electron. The common tangent marks the isostructural phase transition.

the transition temperature to be $T \sim \Delta E/\Delta S = 20$ mRyd$/k_B \ln 6 \sim 1800$ K, which is, however, fairly large.

4. Magnetic studies of CeP

In all of the calculations of the previous section, a ferromagnetic (F) arrangement of cerium moments has been assumed. In order to address the important question of the ground-state magnetic structure of the cerium monopnictides, we have also performed calculations for CeP in the antiferromagnetic arrangements AF1 and AF2 in the rock-salt B1 crystal structure. Specifically, in these two antiferromagnetic structures the cerium moments are ferromagnetically aligned in planes which are then antiferromagnetically stacked in the (100) (AF1) or (111) (AF2) directions. The total energies as functions of the volume are shown in figure 8 for the F, AF1 and AF2 magnetic structures (all in the B1 structural arrangement). It is seen that for one localized f electron per cerium atom the AF1 structure is the ground state. The equilibrium volumes of the three magnetic structures considered in this work are found to be virtually identical. CeP is found to be semimetallic at the minimum-energy position in both the AF1 and AF2 structures, but with negative pressures (expanded volume), a semimetal–semiconductor transition takes place. The evolution of the band gap for these expanded volumes is shown in figure 9. At pressures lower than

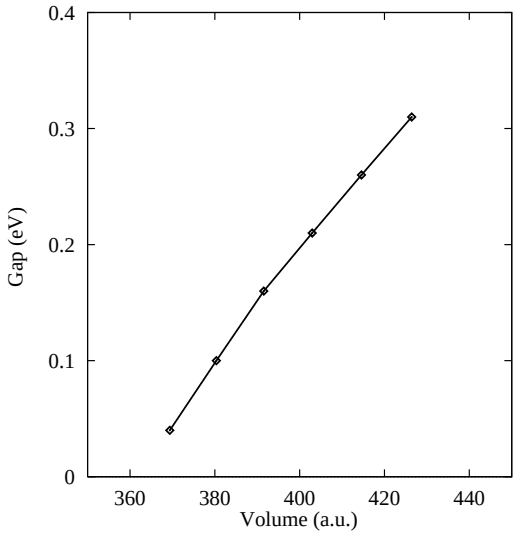

Figure 9. The energy gap in AF1 CeP in eV as a function of volume. The equilibrium volume is 348 a_0^3.

~ -50 kbar (or volumes larger than $\sim 1.08\ V_0$) CeP is a small-gap semiconductor in both the AF1 and AF2 magnetic structures. Again, the negative-pressure regime is not directly accessible experimentally, but might be explored through alloying. At positive pressures, at $\sim$80 kbar, the isostructural transition, in which the f electron changes from being localized to being delocalized, is found. The transition pressure is slightly larger than the value of 71 kbar for the ferromagnetic structure discussed in section 3, due to the fact that the AF1 structure is considered here. On the high-pressure side, the delocalized phase is found to

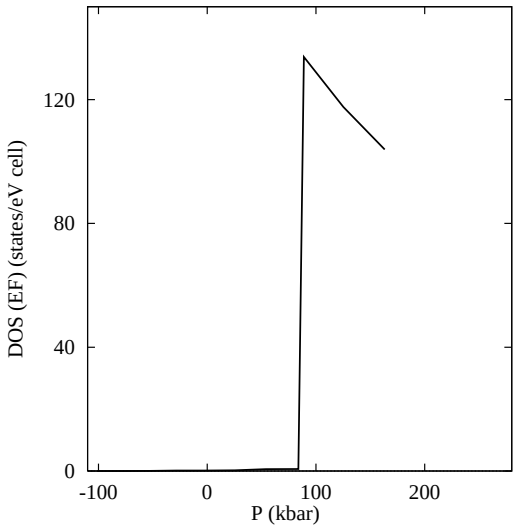

Figure 10. The density of states at the Fermi level in CeP. The occurrence of the isostructural phase transition results in a discontinuous jump.

be paramagnetic, but only just: at slightly higher volumes than that at which the common tangent touches the LSD calculation curve in figure 8, the Ce magnetic moment evolves, with a preference for the AF2 phase. No experimental determination of the magnetic structure of the high-pressure phase has been reported, but the prediction of the present work is that the magnetic structure should change from AF1 below to paramagnetic above the transition line. Below the transition line, the Ce moment in CeP is calculated to be close to 1 μ_B, due to the semimetallic character, with essentially filled P p bands and empty Ce sd bands. The moments at equilibrium volume are found to be 1.04 μ_B, 1.07 μ_B and 1.00 μ_B in the AF1, AF2 and F phases, respectively. The experimental moment is 0.8 ± 0.1 μ_B [17], i.e. significantly lower, because of spin–orbit coupling: the Ce ion is found in its irreducible Γ_7 representation of the $j = 5/2$ spin–orbit multiplet. The observed magnetic structures of the Ce monopnictides are complex, and only for CeP and CeAs do they show AF1 magnetic order. In CeSb and CeBi they are more complex, of the AF1A kind, and we have not performed any calculations for this structure. For CeP, our calculations show that the AF2 structure, which is common for the transition metal oxides, is unfavourable, and the same is true for the ferromagnetic structure for both localized and delocalized f electrons.

5. The electronic band structure and density of states of CeP

The calculated density of states at the Fermi energy is depicted in figure 10 as a function of pressure. Similarly to the magnetic moment, this quantity shows a dramatic jump at the transition from the localized AF1 structure to the delocalized structure. For negative

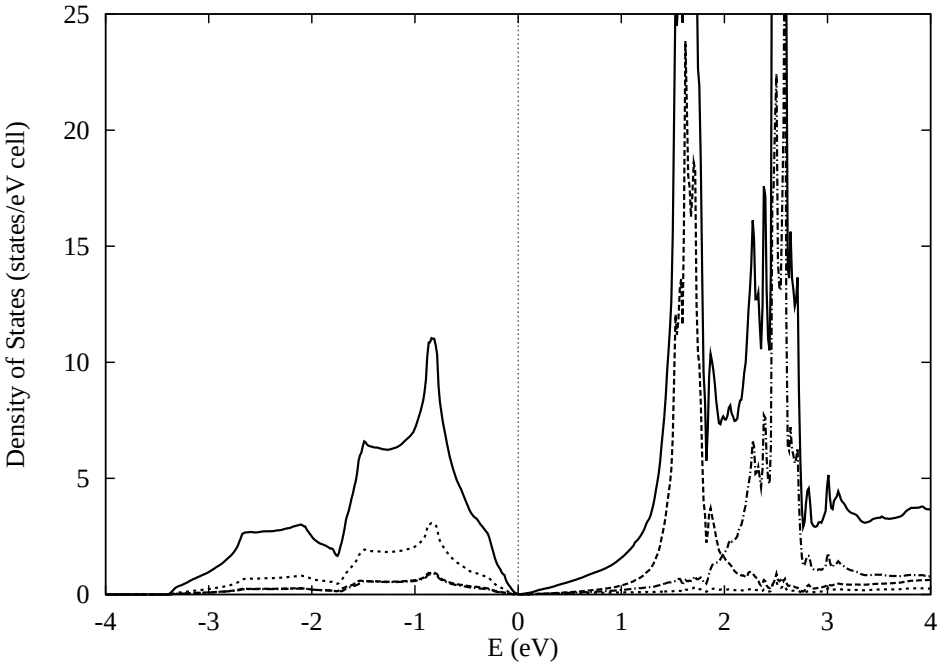

Figure 11. The density of states of CeP in the AF1 magnetic structure and at the experimental lattice constant with one Ce f electron localized. The dashed line marks the Fermi level, which is at zero energy.

and moderate positive pressures the density of states is essentially zero, reflecting the semiconducting or semimetallic character of CeP for these pressures. At the transition pressure the density of states at the Fermi energy reaches its maximum value, which then rapidly decays as the lattice is further compressed. Above the transition pressure of ∼80 kbar our calculation predicts a metallic behaviour in CeP.

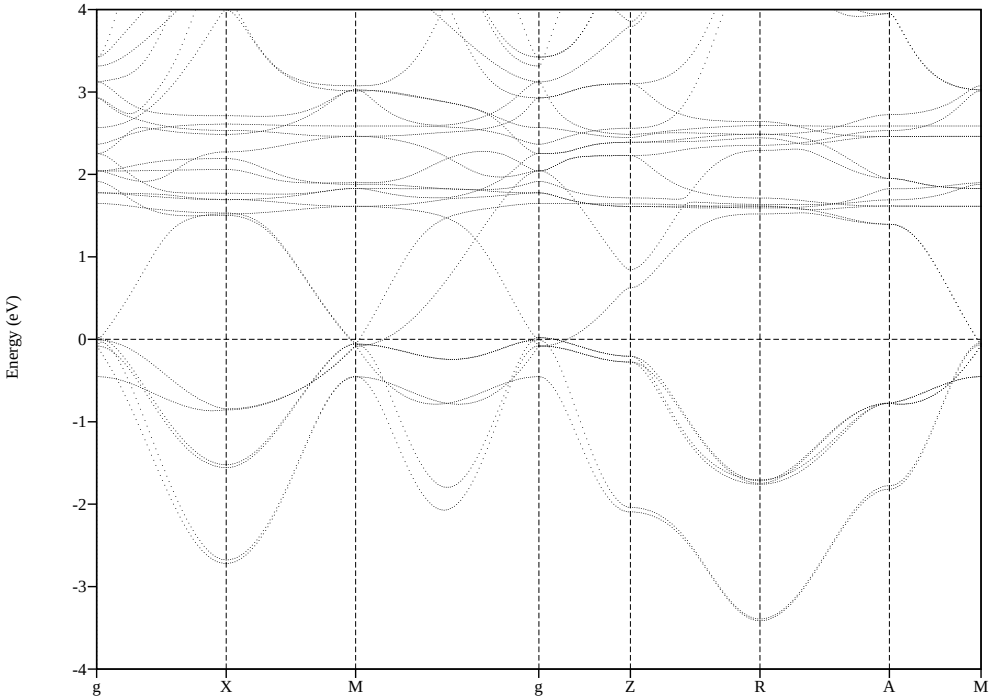

Figure 12. The band structure of CeP in the AF1 magnetic structure and at the experimental lattice constant with one Ce f electron localized. The dashed line marks the Fermi level, which is at zero energy.

The density of states of CeP in the AF1 structure at the equilibrium volume is shown in figure 11. It is characterized by a valence band of predominantly P p character, which is about 3.5 eV wide. The Fermi surface properties are characterized by semimetallic behaviour. The massive peaks in the density of states, at 1.5 and 2.5 eV above the Fermi energy, are the spin-split Ce f levels. Localization of the f electron has taken away the occupied f-electron weight of approximately one electron, which in the LSD approximation (i.e., with delocalized f electrons) is situated in the vicinity of the Fermi energy. This f weight is shifted to well below the bottom of the P p valence density of states, at 7.5 eV below the Fermi energy (not shown in the figure). As a consequence, we have obtained a low density of states of 10^{-2} states eV^{-1}/cell at the Fermi level. Figure 12 shows the CeP band structure calculated at the equilibrium volume in the AF1 magnetic structure. The semimetallic behaviour is seen to originate from small hole pockets around the Γ point in the centre of the Brillouin zone and compensating electron pockets around the M point on the Brillouin zone boundary. These pockets are mostly confined to the basal plane of the Brillouin zone. These results are in accordance with de Haas–van Alphen [23, 24] and photoemission [26] findings as regards the location of the electron and hole pockets.

6. Conclusion

The SIC-LSD total-energy functional provides a complete description of the electronic properties of Ce monopnictides. The equilibrium lattice constants are reproduced with an accuracy of ∼1%, which demonstrates that the self-interaction correction provides the correct energy of f-electron localization. The physical behaviour under hydrostatic pressure is also well reproduced. Transitions from localized to delocalized f electrons are found in all of the Ce monopnictides, and the transition pressures are in good agreement with the experimental values where available. New transitions at higher pressures are predicted. A trend of increasing localization of the f electron is observed with increasing nuclear charge of the ligand, which also causes a volume increase. We note that due to the increasing localization, the f electron in CeSb and CeBi remains localized in the B2 structure. The localization-to-delocalization transitions are calculated to occur at −111 kbar, 71 kbar, 114 kbar, 252 kbar and 370 kbar, respectively in CeN, CeP, CeAs, CeSb and CeBi. In CeN the f electron is delocalized in its ground state. The SIC-LSD functional provides the correct AF1 magnetic ground state for CeP. The energy differences between the F, AF1 and AF2 structures are only a mere 1 mRyd per formula unit. The calculated semimetallic behaviour and the location of the electron and hole pockets in the Brillouin zone are in agreement with experiments.

Acknowledgments

This work has benefited from collaborations within, and has been partially funded by, the Human Capital and Mobility Network on ‘Ab initio (from electronic structure) calculation of complex processes in materials’ (contract: ERBCHRXCT930369). AS acknowledges support from the Danish Natural Science Research Council (Grant No 11-9001-3).

References

[1] Jayaraman A, Lowe W, Longinotti L D and Bucher E 1976 *Phys. Rev. Lett.* **36** 366
[2] Baer Y, Hauger R, Zürcher Ch, Campagna M and Wertheim G K 1978 *Phys. Rev.* B **18** 4433
[3] Franciosi A, Weaver J H, Mårtensson N and Croft M 1981 *Phys. Rev.* B **24** 3651
[4] Gudat W, Rosei R, Weaver J H, Kaldis E and Hulliger F 1982 *Solid State Commun.* **41** 37
[5] Patthey F, Cattarinussi S, Schneider W-D, Baer Y and Delley B 1986 *Europhys. Lett.* **2** 883
[6] Delin A, Oppeneer P M, Brooks M S S, Kraft T, Wills J M, Johansson B and Eriksson O 1997 *Phys. Rev.* B **55** R10 173
[7] Vedel I, Redon A M, Rossat-Mignod J, Vogt O and Leger J M 1987 *J. Phys. C: Solid State Phys.* **20** 3439
[8] Mori N, Okayama Y, Takahashi H, Haga Y and Suzuki T 1993 *Physica* B **186–188** 444
[9] Werner A, Hochheimer H D, Meng R L and Bucher E 1983 *Phys. Lett.* **97A** 207
[10] Leger J M, Vedel I, Redon A M and Rossat-Mignod J 1987 *J. Magn. Magn. Mater.* **63+64** 49
[11] Leger J M, Ravot D and Rossat-Mignod J 1984 *J. Phys. C: Solid State Phys.* **17** 4935
[12] Leger J M, Oki K, Rossat-Mignod J and Vogt O 1985 *J. Physique* **46** 889
[13] The errors in the quoted experimental transition pressures are the present authors’ estimates based on the hysteresis loop observed in the experimental P–V curves. The quoted volume changes are relative to the equilibrium volume and taken at the average transition pressure.
[14] Okayama Y, Ohara Y, Mituda S, Takahashi H, Yoshizawa H, Osakabe T, Kohgi M, Haga Y, Suzuki T and Mori N 1993 *Physica* B **186–188** 531
[15] Hulliger F, Landolt M, Ott H R and Schmelczer R 1975 *J. Low Temp. Phys.* **20** 269
[16] Chattopadhyay T 1994 *Science* **264** 226
[17] Kohgi M, Osakabe T, Kakurai K, Suzuki T, Haga Y and Kasuya T 1994 *Phys. Rev.* B **49** 7068
[18] Suzuki T 1993 *Physica* B **186–188** 347
[19] Suzuki T *et al* 1995 *Physica* B **206+207** 771

[20] Kwon Y S, Haga Y, Nakamura O, Suzuki T and Kasuya T 1990 *Physica* B **171** 324
[21] Takeda N, Kwon Y S, Haga Y, Sato N, Suzuki T and Komatsubara T 1993 *Physica* B **186–188** 153
[22] Kitazawa H, Oguro I, Hirai M, Kondo Y, Suzuki T and Kasuya T 1985 *J. Magn. Magn. Mater.* **47+48** 532
[23] Haga Y, Uesawa A, Terashima T, Uji S, Aoki H, Kwon Y S and Suzuki T 1995 *Physica* B **206+207** 792
[24] Terashima T, Uji S, Aoki H, Joss W, Haga Y, Uesawa A and Suzuki T 1997 *Phys. Rev.* B **55** 4197
[25] Kumigashira H, Yang S-H, Yokoya T, Chainani A, Takahashi T, Uesawa A, Suzuki T, Sakai O and Kaneta Y 1996 *Phys. Rev.* B **54** 9341
[26] Kumigashira H, Yang S-H, Yokoya T, Chainani A, Takahashi T, Uesawa A and Suzuki T 1997 *Phys. Rev.* B **55** R3355
[27] Perdew J P and Zunger A 1981 *Phys. Rev.* B **23** 5048
[28] Temmerman W M, Svane A, Szotek Z and Winter H 1997 *Electronic Density Functional Theory: Recent Progress and New Directions* ed J F Dobson, G Vignale and M P Das (New York: Plenum)
[29] Svane A, Szotek Z, Temmerman W M and Winter H 1997 *Solid State Commun.* **102** 473
[30] Hasegawa A 1980 *J. Phys. C: Solid State Phys.* **13** 6147
[31] Norman M R, Koelling D D and Freeman A J 1985 *Phys. Rev.* B **31** 6251
Norman M R, Koelling D D and Freeman A J 1985 *Phys. Rev.* B **32** 7748
[32] Lim S P and Cooper B R 1991 *J. Appl. Phys.* **70** 5809
Cooper B R, Sheng Q G, Lim S P, Sanchez-Castro C, Kioussis N and Wills J M 1992 *J. Magn. Magn. Mater.* **108** 10
Cooper B R, Lim S P, Avgin I, Sheng Q G and Price D L 1995 *J. Phys. Chem. Solids* **56** 1509
[33] Narita A and Schoenes J 1993 *Physica* B **186–188** 580
[34] Liechtenstein A I, Antropov V P and Harmon B N 1994 *Phys. Rev.* B **49** 10 770
[35] Yaresko A N, Oppeneer P M, Perlov A Ya, Antonov V N, Kraft T and Eschrig H 1996 *Europhys. Lett.* **36** 551
[36] Svane A and Gunnarsson O 1990 *Phys. Rev. Lett.* **65** 1148
[37] Szotek Z, Temmerman W M and Winter H 1993 *Phys. Rev.* B **47** 4029
[38] Temmerman W M, Szotek Z and Winter H 1993 *Phys. Rev.* B **47** 1184
[39] Szotek Z, Temmerman W M and Winter H 1994 *Phys. Rev. Lett.* **72** 1244
[40] Svane A 1994 *Phys. Rev. Lett.* **72** 1248
[41] Svane A and Gunnarsson O 1988 *Phys. Rev.* B **37** 9919
Svane A and Gunnarsson O 1988 *Europhys. Lett.* **7** 171
[42] Majewski J and Vogl P 1992 *Phys. Rev.* B **46** 12 219
Majewski J and Vogl P 1992 *Phys. Rev.* B **46** 12 235
[43] Ishii Y and Terakura K 1990 *Phys. Rev.* B **42** 10 924
Miyazaki T, Ishii Y and Terakura K 1991 *Prog. Theor. Phys. Suppl.* **106** 173
Miyazaki T, Terakura K and Ishii Y 1993 *Phys. Rev.* B **48** 16 992
[44] Manning S M and Edwards D M 1993 *J. Phys.: Condens. Matter* **5** 6203
Edwards D M, Manning S M and Rettke-Grover J 1994 *Phil. Mag.* B **69** 849
[45] Arai M and Fujiwara T 1995 *Phys. Rev.* B **51** 1477
[46] Svane A 1992 *Phys. Rev. Lett.* **68** 1900
[47] Temmerman W M, Szotek Z and Winter H 1993 *Phys. Rev.* B **47** 11 533
[48] Solov'ev I V, Liechtenstein A I and Gubanov V A 1991 *Sov. Phys.–Solid State* **33** 572
[49] Svane A, Trygg J, Eriksson O and Johansson B 1997 *Phys. Rev.* B **56** 7143
[50] Beiden S V, Temmerman W M, Szotek Z and Gehring G A 1997 *Phys. Rev. Lett.* **79** 3970
[51] Svane A and Gunnarsson O 1990 *Solid State Commun.* **76** 851
[52] Hohenberg P and Kohn W 1964 *Phys. Rev.* **136** B864
Kohn W and Sham L J 1965 *Phys. Rev.* **140** A1133
[53] Jones R O and Gunnarsson O 1989 *Rev. Mod. Phys.* **61** 689
[54] Svane A 1995 *Phys. Rev.* B **51** 7924
[55] Svane A 1996 *Phys. Rev.* B **53** 4275
[56] Andersen O K 1975 *Phys. Rev.* B **12** 3060
[57] Andersen O K and Jepsen O 1984 *Phys. Rev. Lett.* **53** 2571
Andersen O K, Jepsen O and Glötzel O 1985 *Proc. Int. School of Physics, Course LXXXIX (Varenna, 1985)* ed F Bassani, F Fumi and M P Tosi (Amsterdam: North-Holland) p 59
[58] Methfessel M 1988 *Phys. Rev.* B **38** 1537
Methfessel M, Rodriguez C O and Andersen O K 1989 *Phys. Rev.* B **40** 2009
[59] Wyckoff R W G 1964 *Crystal Structures* vol 1 (New York: Wiley)